Strongly Interacting Bosons in a Disordered Optical Lattice

M. White, M. Pasienski, D. McKay, S. Q. Zhou, D. Ceperley, and B. DeMarco
Department of Physics, University of Illinois at Urbana-Champaign, Urbana, Illinois 61801, USA
(Received 4 September 2008; published 5 February 2009)

We experimentally probe the properties of the disordered Bose-Hubbard model using an atomic Bose-Einstein condensate trapped in a 3D disordered optical lattice. Controllable disorder is introduced using a fine-grained optical speckle field with features comparable in size to the lattice spacing along every lattice direction. A precision measurement of the disordering potential is used to compute the single-particle parameters of the system. To constrain theories of the disordered Bose Hubbard model, we have measured the change in condensate fraction as a function of disorder strength for several different ratios of tunneling to interaction energy. We observe disorder-induced, reversible suppression of condensate fraction for superfluid and coexisting superfluid–Mott-insulator phases.

DOI: 10.1103/PhysRevLett.102.055301 PACS numbers: 67.85.Hj, 03.75.Lm, 37.10.Jk, 61.43.−j

Disorder is intimately involved in such spectacular effects as the fractional quantum Hall effect and vortex pinning in type-II superconductors. Understanding the role of disorder is therefore of fundamental interest to materials research and condensed matter physics. Universal behavior, such as Anderson localization [1], in disordered noninteracting systems is well understood. However, the effects of disorder combined with strong interactions remains an outstanding challenge to theory. In this work, we study a paradigm for disordered, strongly correlated bosonic systems: the disordered Bose-Hubbard (DBH) model. Despite being applied to many physical systems—from superfluids in porous media to superconducting thin films—questions remain regarding fundamental properties of the DBH model. For example, theoretical work using mean field theory [2–7], renormalization group [8], replica theory [9], and quantum Monte Carlo algorithms [10–15] disagree on the nature of the ground state phase diagram.

While ultracold atom gases are ideal for studying disorder [16], having recently been applied to explore Anderson localization [17,18] and quasicrystalline 1D systems [19,20], the regime of strong interactions and disorder has not been previously accessed. To experimentally realize the DBH model, we add fine-grained disorder to an optical lattice potential using an optical speckle field with features as small as 570 nm. A unique aspect of this system compared with solid state materials is that the disorder strength is continuously tunable by controlling the intensity of the speckle field.

We prepare ^{87}Rb BECs containing $(3.2 \pm 0.6) \times 10^5$ atoms in a 3D cubic optical lattice potential with 406 nm between sites, as described in Ref. [21]. The lattice potential is characterized using a dimensionless parameter s, where the lattice potential depth is sE_R (E_R is the recoil energy at 812 nm). A nearly isotropic harmonic confining potential generated by a magnetic trap and the Gaussian lattice beam profile leads to a range of site fillings, with approximately three atoms per site in the center of the lattice.

Fine-grained disorder is superimposed on the periodic optical lattice potential by passing 532 nm light through a holographic diffuser to generate an optical speckle field [Fig. 1(a)]. The diffuser randomly scatters the light through a 0.5° range of angles, leading to a random distribution of

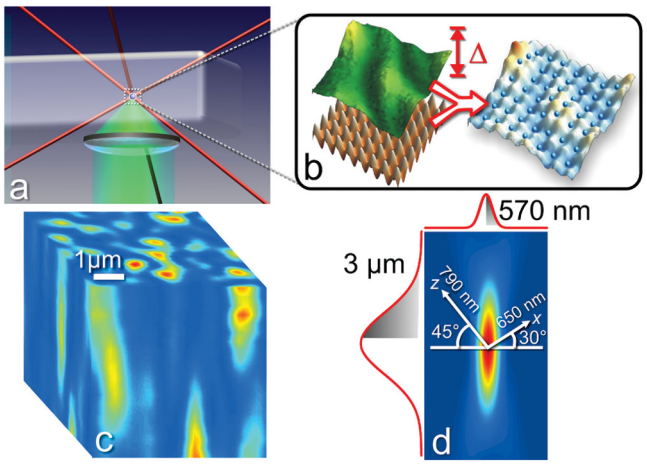

FIG. 1 (color). Fine-grained disorder superimposed on a 3D periodic optical lattice potential. (a) A polycarbonate holographic diffuser (gray disk) is used to create a 532 nm optical speckle field. The light (green) is focused by a 0.9 numerical aperture lens 13 mm from the atoms into the rectangular glass cell, where a BEC (blue circle) is confined in a three-dimensional optical lattice formed from three pairs of counter-propagating 812 nm laser beams (red). (b) The random optical potential (green) created by the optical speckle field adds independently to the lattice potential (red) to create a disordered potential. (c) A sample of the volume of the speckle intensity distribution (shown in false color). (d) The measured speckle intensity is used to reconstruct the AC function (false color). The $1/e^2$ radii of the AC distribution are 570 nm and 3 μm along the transverse and speckle propagation directions; the lattice axes project onto the x and z directions in this plane.

intensities around the focal plane covering a Gaussian envelope with a 160 μm $1/e^2$ radius. Atoms experience a potential energy shift proportional to the intensity of this light, leading to a combined potential that is a disordered lattice potential [Fig. 1(b)]. The average potential energy shift Δ from the speckle field is used to quantify the disorder strength. The dipole force on a 500 nK thermal gas from the speckle-beam envelope is used to calibrate Δ within a 15% systematic uncertainty.

Several previous studies, beginning with Ref. [22], have used speckle to experimentally investigate atoms confined in disordered potentials [17,18,23–25]. Our results are distinguished from prior disordered optical lattice experiments probing the interplay of disorder and strong interactions by the use of fine-grained disorder comparable in length scale to the lattice spacing, which results in weak correlations in the single-particle properties at neighboring lattice sites (typically assumed in theories of the DBH model). In [26], the disorder length scale was nearly an order of magnitude larger than the lattice spacing, giving rise to strong correlations in the disordering potential at nearby sites. Incommensurate lattices were used to create a quasicrystalline system and probe the interacting Aubry-André Hamiltonian in [19]. These quasiperiodic potentials show perfect correlations in measures such as the joint-probability distribution of the disorder-induced energy shift for nearest-neighbor lattice sites.

We achieve the fine-grained disorder limit by using relatively short-wavelength light, a high numerical aperture lens, and a geometry in which the speckle field propagates at 30° and 45° angles to the lattice directions [Fig. 1(a)]. The speckle length scale is characterized using the intensity autocorrelation (AC) function, which was determined by a measurement of the speckle intensity in a $10 \times 100 \times 80$ μm volume using a scanning, high-resolution optical microscope [Fig. 1(c)]. A fit to the measured AC distribution [Fig. 1(d)] to a Gaussian gives 790 and 650 nm $1/e^2$ radii, less than two lattice spacings, along the lattice directions. The shift in energy at nearest-neighbor lattice sites is therefore weakly correlated.

At sufficiently low temperature and high s, atoms in a disordered lattice are described by the DBH Hamiltonian

$$H = \sum_i (\varepsilon_i - \tilde{\mu}_i) n_i - \sum_{\langle ij \rangle} t_{ij} b_i^\dagger b_j + \sum_i U_i n_i (n_i - 1)/2 \tag{1}$$

with site (kinetic and potential) energies ε_i, tunneling energies between nearest neighbors t_{ij}, on-site interaction energies U_i, and effective chemical potential $\tilde{\mu}_i = \mu - kr_i^2/2$ (μ is the chemical potential, k is the spring constant for the parabolic confining potential, and r_i is the distance to the center of the lattice). The disordering potential gives rise to site-dependent distributions for the DBH model parameters ε, t, and U. The site energies are disordered by potential energy shifts, the tunneling energy by changes in the potential barrier between sites, and the interaction energy by modification of the curvature of the potential near the center of each lattice site. We define the tunneling and interaction energies as in Ref. [27], although localized basis functions for each site must be used for the single-particle wave functions in the disordered potential.

In typical theoretical treatments of the DBH model, the disorder is limited to either the site or tunneling energies, which are generally assumed to be uniformly or Gaussian distributed. However, for our system, the statistical properties of the microscopic disorder are completely determined. We numerically compute the distributions for ε, t, and U by calculating the local basis functions on a 3D disordered lattice potential that reproduces the geometry shown in Fig. 1(a); the parabolic confining potential is not included in this calculation. The basis set of single-particle states $w_i(\vec{x} - \vec{x}_i)$ is constructed using imaginary time projection starting from states localized on the sites of the uniform lattice potential: $w_i(\vec{r}) = \langle \vec{r} | \exp(-\tau[-\hbar^2 \vec{\nabla}^2/2m + V(\vec{r})]) | \vec{r}_i \rangle$, where V is the disordered potential. The evolution is terminated when the high energy components are sufficiently suppressed but the basis functions are still well localized. The basis set is then orthogonalized using the Lowdin scheme in order to preserve the localization to the maximal extent [28]. The distributions of $\varepsilon_i = \int w_i^*(\vec{x} - \vec{x}_i)[-\hbar^2 \vec{\nabla}^2/2m + V(\vec{r})] w_i(\vec{x} - \vec{x}_i) d^3\vec{x}$, t_{ij}, and U_i are calculated using this basis set, averaged over 150 random realizations of the speckle field [29].

Computed probabilities for the DBH parameters are shown in Fig. 2. These distributions show that the speckle induces the strongest disorder in t and ε compared with U—the relative scales of the disorder in each parameter are determined by the width of the distributions compared with their mean. We have verified that the width σ_ε of the site energy distribution is proportional to Δ, as expected from

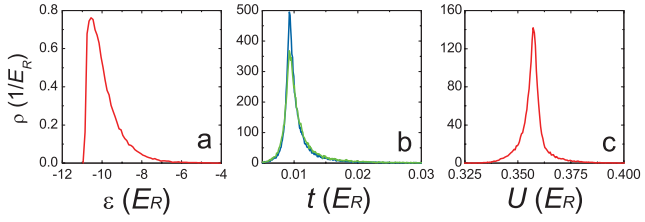

FIG. 2 (color). Probability density ρ of the DBH parameters for $s = 14$ and $\Delta = 1$. The distribution for ε shown in (a) is one-sided, since the blue-detuned speckle potential can only increase the potential energy of a lattice site. In (b), the tunneling energy distributions are computed separately along the x (blue) and z (green) directions. The average of the ratio of tunneling energy along the x and z direction does not deviate by more than 10% even for moderately strong disorder ($\Delta \sim U$). The disorder does not shift the most probable values of t and U, even though the mean values of these parameters change with increasing Δ. The $\Delta = 0$ values are $\varepsilon = -10.85 E_R$, $t = 0.0095 E_R$, and $U = 0.360 E_R$.

the distribution of speckle intensities $P(I) \propto e^{-I/\bar{I}}$ ($\bar{I}$ is the mean intensity and $\Delta \propto \bar{I}$). The similarity of the t distributions shown separately along the x and z directions in Fig. 2(b) confirms that the asymmetry of the speckle field with respect to the lattice directions does not play an important role in the distribution of tunneling energies.

In this Letter, we measure the effect of disorder on condensate fraction, which provides indirect information on the outstanding question of how the SF and MI phases in the uniform lattice transform when disorder is added. In their seminal paper on the DBH model [2], Fisher *et al.* argue that a Bose-glass (BG) phase intervenes between the MI and SF phases, implying that disorder transforms the MI phase into a BG phase. However, recent results using, for example, stochastic mean field [3] and replica theory [9] indicate that disorder can change the MI phase directly into a SF. We do not resolve this issue directly because condensate fraction is related, but not identical, to SF fraction. Only a portion of atoms are condensed because of the strong interactions in the DBH model; the condensate fraction is strictly zero for the MI phase and sufficiently localized BG phases.

Time-of-flight absorption imaging after release from the disordered lattice is used to measure the fraction of atoms in the condensate. The images are fit to the sum of a Thomas-Fermi (TF) profile (for a harmonic trap) and a broader Gaussian; we refer to these as the condensate and noncondensate components, numbering N_0 and N_{nc}, respectively. The noncondensate component may be atoms in MI or BG phases, or atoms in thermally excited states. The condensate component may be atoms in a SF phase, or a BG phase with a long coherence length (i.e., nearly equal to the diameter of the gas); a condensate measured in this fashion does not imply complete coherence across the entire gas. A sample image and corresponding cross-sectional profile are shown as insets to Fig. 3(c). We observe two-component profiles for all lattice depths s and disorder strengths Δ used in this work, and the width of the TF profile changes by less than 20% for the range of Δ in Fig. 3.

The measured condensate fraction $N_0/N = N_0/(N_0 + N_{\mathrm{nc}})$ is shown in Figs. 3(a)–3(c) for $s = 6$, 12, and 14, three lattice depths that span different regimes for the pure Bose-Hubbard (BH) phase diagram. At zero temperature, the BH model with a parabolic confining potential predicts a SF phase with negligible quantum depletion at $s = 6$, a strongly depleted SF phase at $s = 12$, and coexisting MI and depleted SF phases (as nested spherical SF and unit filling MI shells surrounding a SF core) at $s = 14$ [27,30]. For the data in Fig. 3, the condensate fraction before transfer into the disordered lattice is greater than 90%. Data are shown for slow (15 ms) release from the lattice, which is used to measure the degree to which transfer into the disordered lattice is reversible, and fast (200 μs) release (or "band-mapping"), which probes N_0/N in the disordered lattice [31]. The ratio s/Δ is kept fixed both during the turn on and release from the disordered lattice. For slow release, the measured condensate fraction does not depend strongly on the release time, and longer release times do not give higher condensate fraction. Ideally, in the absence of heating during transfer into the disordered lattice, slow release would recover the condensate fraction prior to transfer.

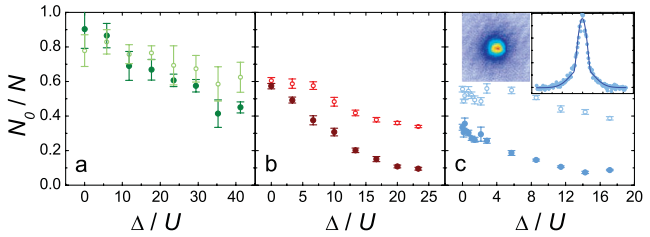

FIG. 3 (color). Measured condensate fraction N_0/N in the disordered lattice potential. Data are shown for $s =$ (a) 6, (b) 12, and (c) 14. The disorder strength normalized to U corresponds to $\Delta = 0$–$7E_R$ for (a) and (b) and $\Delta = 0$–$6E_R$ for (c). The hollow (solid) points are the condensate fraction after slow (fast) release from the lattice. Each data point is the average of more than six measurements at fixed Δ and s; the error bars show the statistical uncertainty. The inset to (c) is an image with a 400 μm field-of-view at $s = 14$ and $\Delta = 2E_R$ ($\Delta/U = 5.7$). The cross-sectional profile of this image shows the fit to a two-component distribution (solid line) used to determine N_0/N. We used an empirical imaging noise model to determine that the systematic error in measurements of low N_0/N was less than 0.03.

We observe that disorder leads to partially reversible changes in condensate fraction. We interpret the irreversible decrease in N_0/N measured for sufficiently large Δ as an increase in heating during transfer into the disordered lattice. This heating is never so strong that the condensate is destroyed; the lowest measured condensate fraction for slow release is 0.34 at $s = 12$ and maximum Δ. We were not able to determine the source of this heating, which may result from vibration of the speckle field relative to the lattice potential or long adiabatic time scales related to the disappearance of the band gap for strong disorder. A calculation of the density of states using the basis set constructed on the disordered lattice indicates that the gap between the ground and first excited band disappears for approximately $\Delta = 0.8$, 1, and $1.75E_R$ (corresponding to $\Delta/U = 4.7$, 3.3, and 5) for $s = 6$, 12, and 14.

The significant reversible changes in N_0/N evident in the fast release data in Fig. 3 may be caused by adiabatic transformations between phases induced by the disorder and by quantum depletion induced by interactions between atoms. Quantum depletion in the pure lattice at zero temperature is anticipated to be significant for $s = 12$ and 14; site-decoupled mean field theory predicts $N_0/N = 0.97$, 0.64, and 0.36 at $s = 6$, 12, and 14 for our system (the ratio of atoms in the SF to MI phase is 0.83 at $s = 14$)[32].

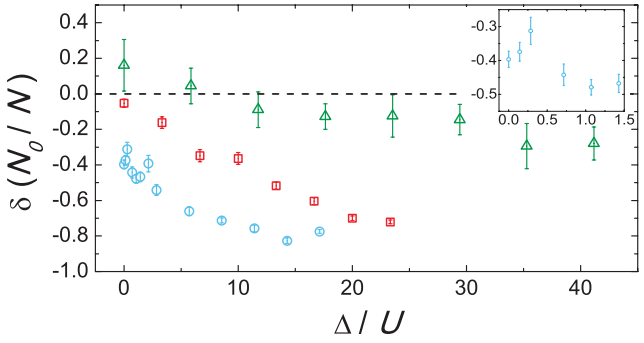

FIG. 4 (color). The reversible change in condensate fraction induced by disorder. Data are shown for $s = 6$ (green triangles), $s = 12$ (red squares), and $s = 14$ (blue circles). Each data point is derived from a pair of slow and fast release points from Fig. 3; the errors bars are computed using the statistical uncertainties from Fig. 3. An effect unrelated to disorder is the reduction in N_0/N for $s = 14$ and $\Delta = 0$, which reflects the presence of atoms in the MI phase in the pure lattice. The inset is an expanded view of the low Δ/U data for $s = 14$.

Because the disorder does not significantly affect the interaction energy (and therefore is not likely to impact quantum depletion), the systematic reduction of N_0/N as Δ is increased for the fast release may be an indication that disorder is inducing a transformation between quantum phases.

To isolate the effect of the disordered lattice on condensate fraction from changes caused by heating, we define the reversible fractional change in N_0/N as $\delta(N_0/N) = (N_0/N)_{\text{fast}}/(N_0/N)_{\text{slow}} - 1$, which is shown in Fig. 4 for each pair of slow and fast release data points in Fig. 3. If disorder results in no change in N_0/N or in a change entirely due to heating, then $\delta(N_0/N) = 0$, which is indicated by the dashed line on Fig. 4. The reversible reduction in condensate fraction evident in Fig. 4 at all lattice depths is more pronounced at higher s and saturates above $\Delta/U = 15$ for $s = 14$.

The inset to Fig. 4 shows an expanded view at low Δ for $s = 14$. Data taken in this regime are sensitive to the effect of weak disorder on the unit filling MI phase. We observe that for relatively weak disorder at $s = 14$, approximately a 10% reversible decrease in N_0/N is measured up to $\Delta/U = 1$ (with no change in N_0/N after slow release). This result may seem to be at odds with predictions that disorder will transform the MI into SF in this regime [3,9]. However, these data are consistent with several scenarios for the effect of weak disorder on the MI phase, including transformation into a depleted SF phase such that N_0/N is unchanged, or conversion into a BG phase with a long enough correlation length such that the momentum distribution is not strongly affected. Before a detailed comparison with these data will be able to constrain theory, finite temperature and the distribution of DBH model parameters shown in Fig. 2 must be included in calculations of condensate fraction. Furthermore, Eq. (1) requires corrections for multiple bands at the highest values of Δ.

In conclusion, the data in this manuscript may be used as a benchmark for predictions—N_0/N can be straightforwardly computed in many theoretical approaches. In contrast to condensed matter systems, for which microscopic disorder cannot be fully characterized, we have completely computed the DBH model parameters for the disordered lattice, thereby eliminating the disorder as a free parameter in theory. The techniques we employ may also be used to study disorder in the (Fermi) Hubbard model, which is of interest to the high-temperature superconducting cuprates.

This work was funded by the ARO, the NSF, the DARPA OLE program, and the Sloan Foundation.

[1] P. W. Anderson, Phys. Rev. **109**, 1492 (1958).
[2] M. P. A. Fisher *et al.*, Phys. Rev. B **40**, 546 (1989).
[3] U. Bissbort *et al.*, arxiv:0804.0007.
[4] P. Buonsante *et al.*, Phys. Rev. A **76**, 011602(R) (2007).
[5] B. Damski *et al.*, Phys. Rev. Lett. **91**, 080403 (2003).
[6] K. Sheshadri *et al.*, Phys. Rev. Lett. **75**, 4075 (1995).
[7] K. V. Krutitsky *et al.*, New J. Phys. **8**, 187 (2006).
[8] K. G. Singh *et al.*, Phys. Rev. B **46**, 3002 (1992).
[9] J. Wu and P. Phillips, Phys. Rev. B **78**, 014515 (2008).
[10] K. G. Balabanyan *et al.*, Phys. Rev. Lett. **95**, 055701 (2005).
[11] N. Prokof'ev *et al.*, Phys. Rev. Lett. **92**, 015703 (2004).
[12] W. Krauth *et al.*, Phys. Rev. Lett. **67**, 2307 (1991).
[13] J. Kisker *et al.*, Phys. Rev. B **55**, R11 981 (1997).
[14] P. Sengupta *et al.*, New J. Phys. **9**, 103 (2007).
[15] R. T. Scalettar *et al.*, Phys. Rev. Lett. **66**, 3144 (1991).
[16] M. Lewenstein *et al.*, Adv. Phys. **56**, 243 (2007).
[17] G. Roati *et al.*, Nature (London) **453**, 895 (2008).
[18] J. Billy *et al.*, Nature (London) **453**, 891 (2008).
[19] L. Fallani *et al.*, Phys. Rev. Lett. **98**, 130404 (2007).
[20] J. E. Lye *et al.*, Phys. Rev. A **75**, 061603(R) (2007).
[21] D. McKay *et al.*, Nature (London) **453**, 76 (2008).
[22] J. E. Lye *et al.*, Phys. Rev. Lett. **95**, 070401 (2005).
[23] D. Clement *et al.*, New J. Phys. **8**, 165 (2006).
[24] Y. P. Chen *et al.*, Phys. Rev. A **77**, 033632 (2008).
[25] D. Clement *et al.*, Phys. Rev. A **77**, 033631 (2008).
[26] T. Schulte *et al.*, Phys. Rev. Lett. **95**, 170411 (2005).
[27] D. Jaksch *et al.*, Phys. Rev. Lett. **81**, 3108 (1998).
[28] J. G. Aiken *et al.*, Int. J. Quantum Chem. **18**, 1101 (1980).
[29] S. Q. Zhou and D. Ceperley (to be published).
[30] B. DeMarco *et al.*, Phys. Rev. A **71**, 063601 (2005).
[31] M. Greiner *et al.*, Phys. Rev. Lett. **87**, 160405 (2001).
[32] K. Sheshadri *et al.*, Europhys. Lett. **22**, 257 (1993).